Giuni, M., Benard, E., and Green, R. (2010) Near field structure of wing tip vortices. In: Experimental Fluid Mechanics Conference, 24-26 Nov 2010, Liberec, Czech Republic.

Copyright © 2010 The Authors

A copy can be downloaded for personal non-commercial research or study, without prior permission or charge

The content must not be changed in any way or reproduced in any format or medium without the formal permission of the copyright holder(s)

When referring to this work, full bibliographic details must be given

http://eprints.gla.ac.uk/78902/

Deposited on: 1 May 2013

Enlighten – Research publications by members of the University of Glasgow
http://eprints.gla.ac.uk

NEAR FIELD CORE STRUCTURE OF WING TIP VORTICES

Michea GIUNI*, Emmanuel BENARD†, Richard B. GREEN‡

***Abstract**: High spatial resolution experiments in the near field of a trailing vortex using a Stereoscopic Particle Image Velocimetry technique have been carried out. A NACA 0015 model with flat tip has been tested for several Reynolds numbers and angles of attack.*
An axisymmetric meandering of the vortex is observed and a discussion on the aperiodicity correction method has identified the helicity peak as the most convenient indicator of the vortex centre. The axial velocity in the centre of the vortex has been recorded always as an excess except for low angle of attack cases where intermittent peaks of excess and deficit are superimposed on a large patch of deficit velocity.
The double vortex structure and the consequent double inflection in the tangential velocity profiles is also studied with reference to a vortex age parameter. At already 2 chords of distance from the trailing edge the profiles exhibit axisymmetric behaviour. A spiral structure of the vortex core has been reported as effect of the early stage of the rolling up and considerations on the rotation confirmed the high dependency of the initial phase of the rolling up with the tip shape. The square tip produces a strong asymmetry of the vortex core and an intense secondary vortex.
Good agreement of the tangential velocity and the circulation profiles between the experiments and analytical vortex expressions has been observed. The results confirm the existence of a three-part vortex structure, namely an inner, a logarithmic and an outer region of the vortex where the former is affected by the initial vortex structure and the latter is not universal but shows a dependence on the angle of attack.

1 INTRODUCTION

Wing tip vortices have been intensively studied for more than four decades. Although being a very classical, almost canonical, flow case, a full understanding of the links between the numerous features that this flow exhibits is still lacking. The coexistence of boundary layer separation, high turbulence level, vorticity sheet rolling up, multiple vortices, diffusion, decay, collapse, instability of vortices have been attracting attention of generations of researchers. For example, a proved method to characterize and control wake vortices is not available[7]. Wing tip vortices are of significant importance with respect to the problems associated with their presence: the noise generation in helicopters blades or the cavitation on propellers blades, or the hazard in following aircrafts. One of the main purposes of the research in wing tip vortices is therefore to minimize the effects of the vortex, by accelerating its decay.

The initial roll up of the vortex already appears on the wing surface and the wing tip geometry plays a significant role in this process. While the cross flow boundary layer separation on rounded wing tips always occurs on the suction surface, for flat tip the separation is fixed by the geometry since the flow has to turn more abruptly over the sharp wing tip[6]. Satellite vortices surrounding the main vortex have been detected in the near field[2] and a strong secondary vortex has been observed more frequently in the high angle of attack cases[21].

The problem of the wandering of the vortex has been well acknowledged although the emergence of this phenomena is not clearly identified as it is thought to be emerging from combination of freestream turbulence, unsteadiness arising from the model or multiple vortices. Vortex wandering causes a certain amount of

*Michea Giuni, Aerospace Department, James Watt Building (South), University of Glasgow, Glasgow G12 8QQ, UK. mgiuni@eng.gla.ac.uk
†Emmanuel Benard, Department of Aerodynamics, Energetics and Propulsion, ISAE, 31055 Toulouse cedex 4, FRANCE. emmanuel.benard@isae.fr
‡Richard B. Green, Aerospace Department, James Watt Building (South), University of Glasgow, Glasgow G12 8QQ, UK. richardg@aero.gla.ac.uk

apparent turbulence[19] and various procedures have been developed to correct vortex flow measurements for the resulting biasing effects. For one-point measurements, Devenport et al.[5] proposed a mathematical description of the wandering effects, the results of which provide methods for determining the amplitude of wandering and reversing those effects. For global measurements, such as PIV, the basic idea of all the methods developed is to collocate the centre of the tip vortex in each of the instantaneous velocity measurements frames before averaging[18]. The challenge therefore with this process is to identify a unique property of a tip vortex that can be used to define its center. Different methods have been used and Ramasamy et al.[18] compared the uncorrected measures with five vortex centre detection methods: centroid of vorticity, peak axial velocity, helicity minimum, zero in-plane velocity and Q-criterion. It was found that the method that best describes both the in-plane and out-of-plane quantities is the helicity aperiodicity correction because it includes all the velocity components in its calculation. In their cases the vortex centre axial velocity was always detected as a deficit.
The swirl or tangential velocity of a wing tip vortex has been widely studied focusing especially on the far field where the vortex structure is well defined. An analytical study by Phillips[15] led to the identification of three regions in the vortex based on the tangential velocity. Studies on the near field, and on the vortex formation and development have shown the sensible dependence from the tip geometry[6] and McAlister et al.[14] recorded a double inflection before the peak is reached that is suggested to be caused either by a secondary vortex which produced a second undulation, also detected in the pressure distribution near the wing or by the crossing of the wing shear layer as it wraps around the trailing vortex. This distortion completely disappears within one chord of distance from the trailing edge.
Because of the vortices are sensitive to even very small intrusive probes, combined with the presence of strong unsteadiness of the core flow, the small vortex core dimension and the core structure, Green[8] pointed out that the measuring technique to be adopted has to be global and non-intrusive or local, non-intrusive with conditional sampling. If the effects of the seeding are neglected, that is true in most of the cases (see Adrian et al.[1] or Raffel et al.[17] for particles dynamic), PIV technique respects the criteria of globality and non-intrusivity. The amount of data obtained in a PIV and its processing require a comparable time and disk space resources with CFD simulations. A careful choice and validation of the key aspects is therefore very important to know the accuracy and the reliability of the tests.

2 Experimental arrangement

The experiments were conducted in the low-speed Argyll wind tunnel, a large closed-return facility at the University of Glasgow of dimensions 2.65 m wide by 2.04 m high by 5.60 m long test chamber. The model tested was a NACA 0015 wing of 0.42 m of chord, 1.4 m of span and rectangular wing tip (see Fig. 1). This configuration allows tests with small wall interference and blockage effects.

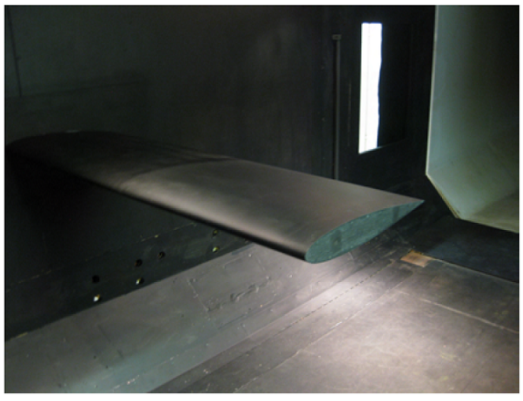

Figure 1: Wing model.

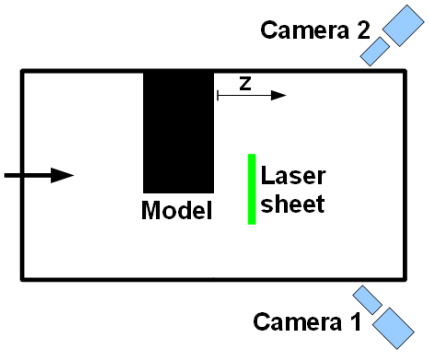

Figure 2: Experimental arrangement.

The model, slid through the test chamber side wall, was mounted on an adjustable plate which allowed the angle of attack and the model height to be adjusted. The wing was positioned in the middle height of the test section and the tip was along the centerline. Tests variables Reynolds numbers of $1 \cdot 10^5$, $5 \cdot 10^5$ and $10 \cdot 10^5$ have been tested at angles of attack of the wing of $4°$, $8°$, $12°$ and $15°$, at wake plane locations $z = 0.25$, 0.5, 1 and 2 chords from the trailing edge and perpendicular to the freestream velocity. The right-hand reference

system origin was on the wing tip trailing edge with x as spanwise coordinate, y vertically directed upwards and z coordinate along the freestream direction.
Two CCD cameras of 11 Mpixels were mounted on the sides of the test section on tripods uncoupled from the wind tunnel (see Fig. 2). Angular stereoscopic system in Scheimpflug condition, as described by Zang and Prasad[20], were adopted with angles between the camera and the object plane round $35°$. This value maintains acceptable levels the errors for evaluations of both the in-plane and out-of-plane velocity component[13]. A double-frame/single-pulse method[12] was used so that for each time step two images were recorded for each camera corresponding to two different laser pulses. Each test consisted in the acquisition of sets composed by 121 two images pairs at a constant frequency of 2 Hz. Tests on the laser pulses delay were performed identifying the values of 15, 35 or 180 μsec (corresponding to the three Reynolds numbers). The light source of the laser sheet was provided by a double cavity Nd:YAG green laser. A laser guiding arm was installed on a rail placed above the test section that allowed two axis translations and three axis rotations of the laser. The laser sheet, of 3 mm of thickness, passed through a window on the top of the test section. The calibration of the cameras, the image acquisition, the laser control and the cross-correlation were accomplished by DaVis 7.2 software distributed by LaVision. A calibration plate of 300 mm by 300 mm with dots in known positions and grooves to calibrate third dimension displacements was used. Every time the laser sheet was moved, a new adjustment of cameras (angles and separation) and a new calibration was performed. A stereo cross-correlation of the image pairs were accomplished by a double step process on an interrogation window of 64 by 64 pixels with 25% of overlap followed by other two steps with interrogation window of 32 by 32 pixels with 50% of overlap leading to the calculation of 53300 vectors per frame and a spatial resolution of the order of 1 mm. The processed data were stored in an external hard disk of 1.5 TBytes.
The flow was seeded with olive oil particles by an Aerosol Generator PivPart40 serie installed at the end of the test section. The nominal peak in the probability density function of the particles size distribution is at 1 μm that corresponds, following the procedure described by Adrian[1], to a particle diameter between 1 and 2 pixels which is what was suggested by Prasad et al.[16]

3 RESULTS AND DISCUSSION

A discussion on the problem of the centering of the vortex is first presented in order to assess the best aperiodicity correction method. Tangential velocity profiles in the near wake are then compared and the double inflection is discussed with reference to a vortex age parameter used to compare profiles. The spiral structure of the vortex core is then illustrated and an estimation of the rotation of the vortex in the initial phase is discussed. Lastly, a comparison of the dimensionless experimental tangential velocity and circulation profiles with the Batchelor analytical vortex is shown.

3.1 VORTEX WANDERING AND CENTERING

Different flow models have been introduced in the years in order to define a vortex but a universal definition has not been agreed yet[9]. Because the vortex moves around, a vortex centre identification method should be used before the time series averaging. The availability of instantaneous three components velocity fields on a plane leads to basic and intuitive vortex centre definitions. It is seen that more sophisticated definitions are not needed in this case where the differences are of few percent of the chord.
In Figure 3, are reported the instantaneous contours of the flow properties used for the identification of the vortex centre for a test case: the cross-plane vorticity component which is the only component that is possible to evaluate with these vector fields; the cross-plane velocity component which, most of the cases, a velocity excess region has been found in the vortex core; the cross-plane helicity component and the sum of the in-plane velocity component with streamlines.
The vortex centre identification is then moved to the finding of the minimum of the in-plane velocity component, the axial velocity peak (either greater or less then the asymptotic velocity) or the minimum vorticity and helicity. In Figure 4 the instantaneous vortex centre positions identified with the four methods are reported for one of the cases studied. A symmetric distribution of the vortex wandering of the order of one tenth of the chord is observed. No preferential direction is observed and the acquisition at 2 Hz precludes a vortex movement frequencies study. Furthermore, although the average position with the different centering methods is very similar, a different vortex wandering history is observed and a different averaged vortex profile is then expected.
The helicity method is preferable because it is the only method that uses all the velocity components. Furthermore, the peakedness of the profile around the centre is higher than what is found with the vorticity method (i.e. higher gradients) which ensures a more precise peak identification.

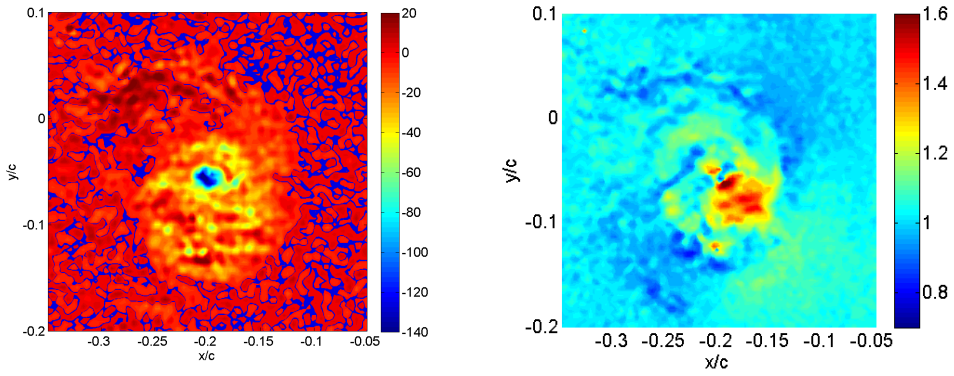

(a) Vorticity.

(b) Cross velocity.

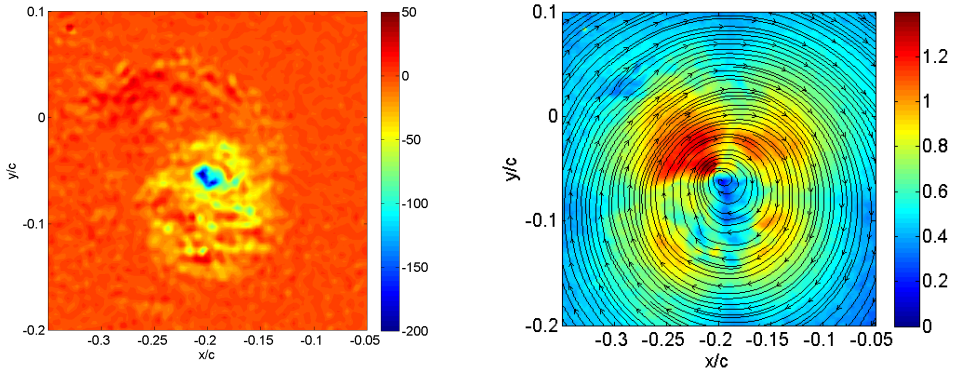

(c) Helicity.

(d) $|u| + |v|$ and streamlines.

Figure 3: Instantaneous contours at $z/c = 0.5$, $Re = 5 \cdot 10^5$, $AoA = 12°$.

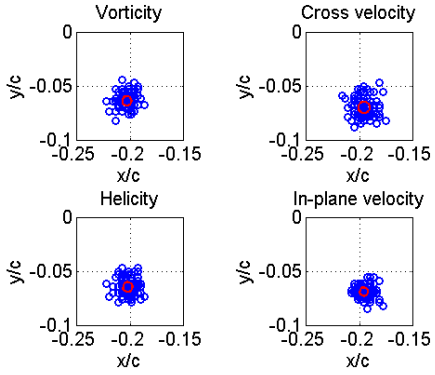

Figure 4: Instantaneous vortex centre positions at $z/c = 0.5$, $Re = 5 \cdot 10^5$, $AoA = 12°$.

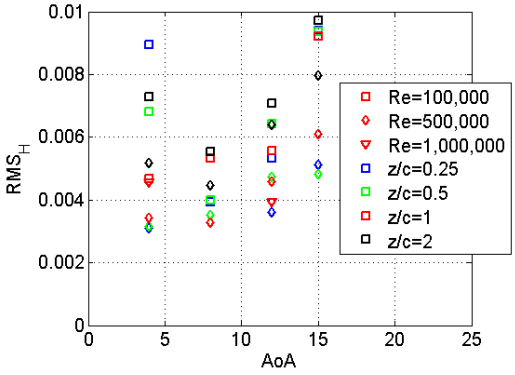

Figure 5: Vortex position RMS non-dimensionalized by the chord.

The origin of meandering can be attributed to several mechanism which co-operate and compete[11]: interference with wind tunnel unsteadiness, excitation of perturbations in the vortex cores by turbulence contained in the wake including satellite vortices, vortex instabilities, propagation of unsteadiness originating from the model. In Figure 5, the root mean square of the distances between instantaneous and helicity method averaged centre position for all the cases are plotted. A general increase of wandering with the increase of the angle of attack is observed at the exception of the high values for the low angle of attack cases which could be attributed to the presence of intense secondary vortices[21]. A fluctuation of few percent of the chord is observed and the RMS values stay below 1%.

The low Reynolds number tests give a higher fluctuation level then the other Reynolds number probably because they are more affected by freestream turbulence. Furthermore, no distance from the model effect is seen in this range. Other PIV experimental results on vortex meandering rms values have been presented by Zuhal and Gharib[21] and by De Souza and Faghani[19] which confirm that there is no general trend in the fluctuations with the increase of the plane location in the wake. Their results also well fit to the conclusion that at very low angles of attack the fluctuations are higher then at high angles of attack because the presence of strong satellite vortices which intensity is comparable to the primary vortex.
It is highlighted in Figure 6 that for low angles of attack, the search of the axial velocity peak (either as excess of deficit with respect to the freestream velocity) is very critical because the vortex core appears as an island of low velocity with subregions of comparable excess and deficit velocity which rotates with the centre. This leads to a non-unique axial velocity peaks and a strong dependency on the searching technique. At the contrary, at high angles of attack, the peak (velocity excess) is well defined and much more intense then the velocity deficit regions around it. The use of the axial velocity method is preferable when the study is focused on the axial velocity itself because it leads to higher and more defined peaks with the limit of questionable results at low angles of attack.

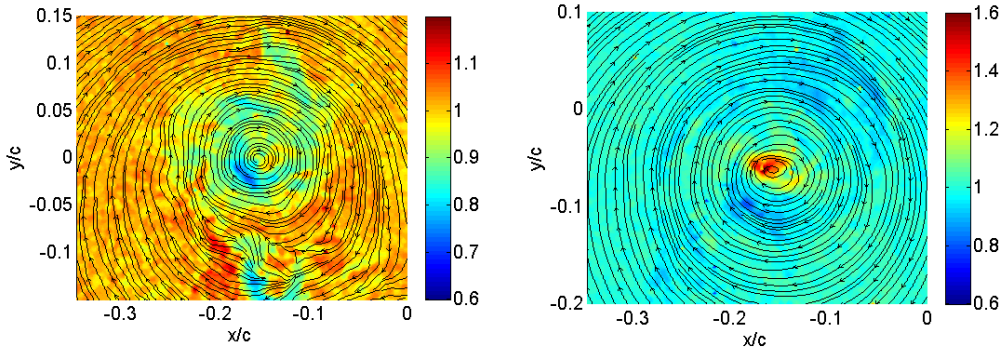

(a) $z/c = 1$, $Re = 1 \cdot 10^5$, $AoA = 4°$.

(b) $z/c = 1$, $Re = 1 \cdot 10^5$, $AoA = 12°$.

Figure 6: Instantaneous axial velocity contours and streamlines.

3.2 DOUBLE INFLECTION AND VORTEX AGE

Tangential velocity profiles as function of the radius are plotted as average of 36 cuts around the vortex. As discussed earlier, the helicity based correction method is used.
In Figure 7, the average velocity profile for the three Reynolds numbers tested at two angles of attack is plotted. The profiles at Reynolds number of half and one million appear very similar. For the low angle of attack case (Fig. 7a), the low Reynolds number shows a second inflection in the velocity profile much stronger then the other Reynolds numbers and a resulting vortex core radius much higher (commonly defined as the radius where the maximum tangential velocity is observed). The averaged contours of the tangential velocity at low angle of attack in Figure 8 show a wider high tangential velocity region for the low Reynolds number (that is a wider vortex core) and at both the contours a strong asymmetry is observed. The axial velocity contours show a stronger boundary layer, a more evident tail in the North region of the vortex and a higher centre peak for the high Reynolds number.
A stronger second inflection for the low Reynolds number cases can be seen also for the high angle of attack in Figure 7b. Figure 9 shows 36 profiles along 36 cuts around the vortex centre at 10 degrees of spacing and the corresponding averaged profile that is what is also reported in Fig. 7b. A strong asymmetry is observed where changing the direction of the cut, the profiles radically change in shape and in the maximum tangential velocity radius. It is clear then the importance and the need of considering several profiles in the description of the vortex structure in the near field. The high tangential velocity contour region in Figure 10 is wider in the low Reynolds case although the differences are less evident then in the low angles of attack. The axial velocity contour remains the same when changing the Reynolds number.
The double inflection type profile is believed to be caused by the superimposition of effects of an intense counter rotating secondary vortex moving around the primary one and by the rolling up of the boundary layer

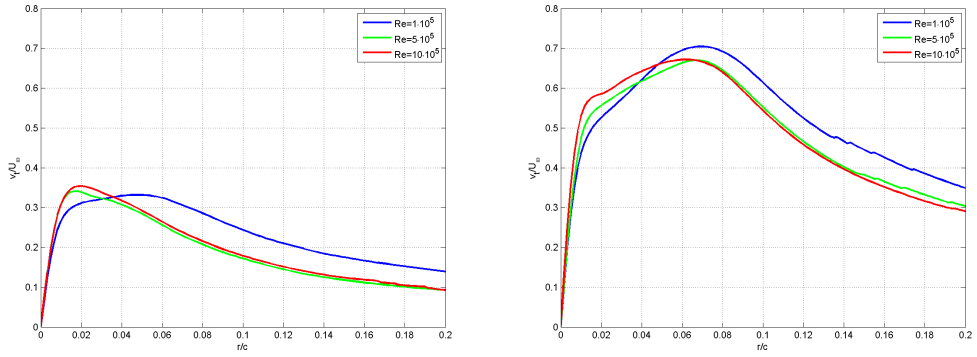

(a) $AoA = 4°$. (b) $AoA = 12°$.

Figure 7: Tangential velocity profiles at $z/c = 1$ as function of the Reynolds number.

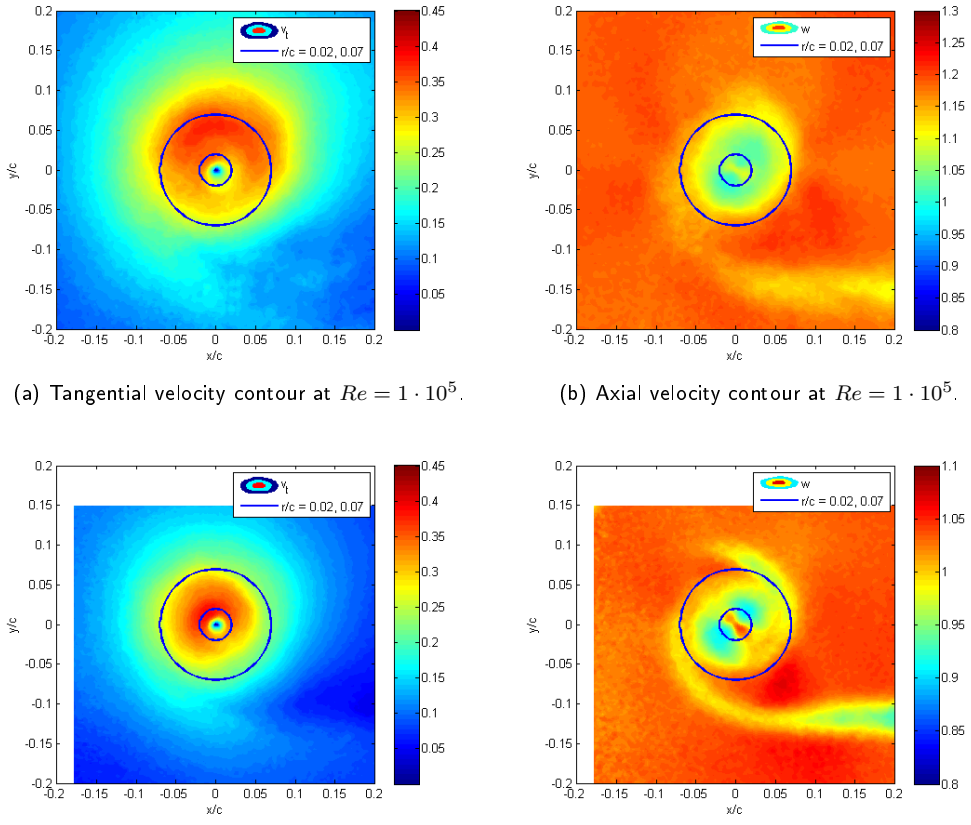

(a) Tangential velocity contour at $Re = 1 \cdot 10^5$. (b) Axial velocity contour at $Re = 1 \cdot 10^5$.

(c) Tangential velocity contour at $Re = 10 \cdot 10^5$. (d) Axial velocity contour at $Re = 10 \cdot 10^5$.

Figure 8: Contours at $z/c = 1$ and $AoA = 4°$.

and the wake. The secondary peak vanishes at already 2 chords of distance from the trailing edge and it is directly related to the geometry of the tip. An abrupt geometry, such as the square tip, forces the tip crossing boundary layer to separate and creates an intense secondary vortex.
An important aspect that needs to be taken into account when comparing these results is that the Reynolds number was changed by the change of the freestream velocity. Keeping the same plane of measurement, the Reynolds number effects and the vortex age effects are added together. In order to try to separate these

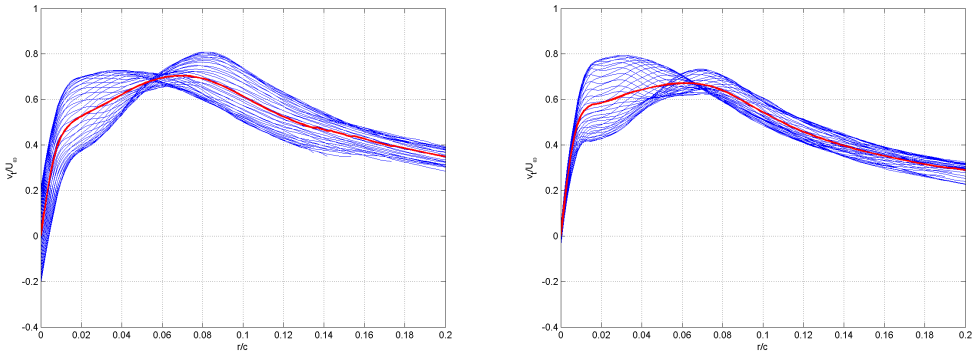

(a) $Re = 1 \cdot 10^5$. (b) $Re = 10 \cdot 10^5$.

Figure 9: Tangential velocity profiles at $z/c = 1$ and $AoA = 12°$.

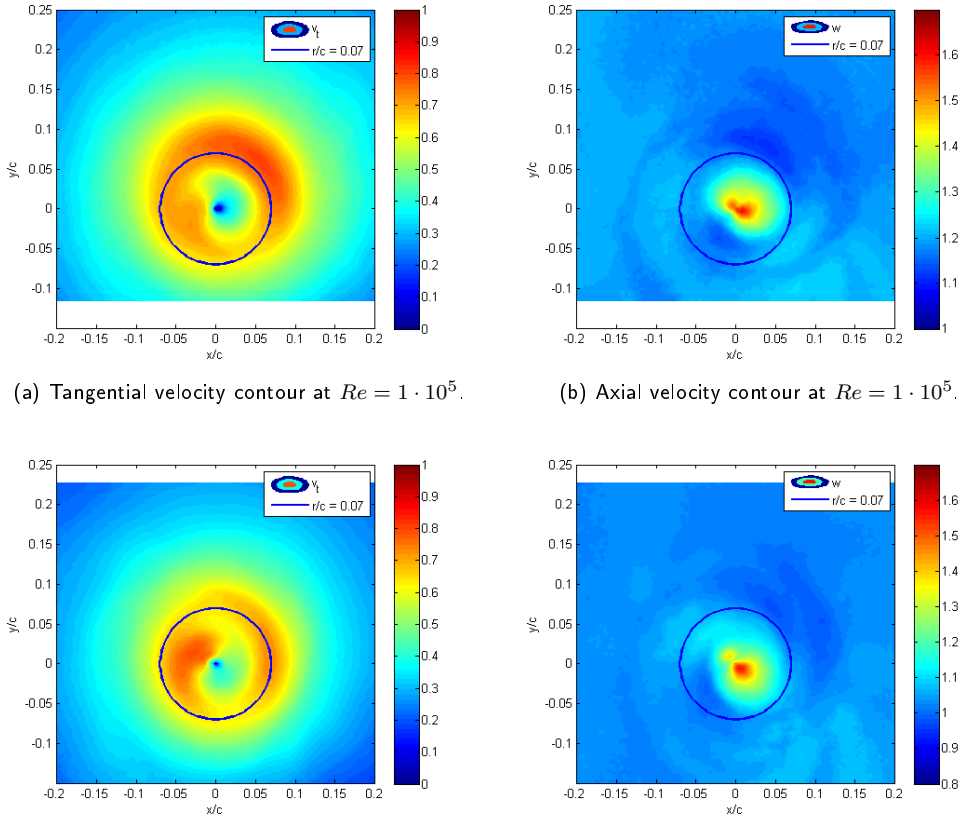

(a) Tangential velocity contour at $Re = 1 \cdot 10^5$. (b) Axial velocity contour at $Re = 1 \cdot 10^5$.

(c) Tangential velocity contour at $Re = 10 \cdot 10^5$. (d) Axial velocity contour at $Re = 10 \cdot 10^5$.

Figure 10: Contours at $z/c = 1$ and $AoA = 12°$.

different effects, the vortex age parameter t^* which has been introduced by Gerz et al.[7] is evaluated:

$$t^* = \frac{z\Gamma_\circ}{U_\infty 2\pi b_\circ^2} \simeq \frac{z\Gamma_V}{U_\infty 2\pi b^2} \tag{1}$$

where z is the streamwise location of the plane (the origin is at the trailing edge), $\Gamma_\circ$ is the wing circulation at the mid-span (root), U_∞ the freestream velocity and $b_\circ$ the initial spacing between the two trailing vortices. With the intent to compare the age parameter of the reported cases, the vortices spacing is substituted by the

wing span b (reasonable in the near wake) and the root circulation is substituted by the vortex circulation Γ_V evaluated by integration of the averaged tangential velocity profile around the vortex at $r/c = 0.24$ (position where an asymptotic value is observed).
In Tab. 1 the vortex age parameter is reported for each of the previous cases. The age of the low Reynolds number cases results higher then the other two that are very similar. Furthermore, for the low angle of attack cases the relative difference in time is much higher then the high angle of attack.

	$\boldsymbol{AoA = 4°}$	$\boldsymbol{AoA = 12°}$
$\boldsymbol{Re = 1 \cdot 10^5}$	$2.66 \cdot 10^{-3}$	$6.58 \cdot 10^{-3}$
$\boldsymbol{Re = 5 \cdot 10^5}$	$1.74 \cdot 10^{-3}$	$5.80 \cdot 10^{-3}$
$\boldsymbol{Re = 10 \cdot 10^5}$	$1.72 \cdot 10^{-3}$	$5.56 \cdot 10^{-3}$

Table 1: Vortex age parameter.

These results confirm what was suggested before, that the comparison between these cases should be made not only taking into account the Reynolds number but also the age of the vortex. Whether the parameter suggested by Gerz et al.[7] is a complete parameter or not is a matter of study and in their work, a number of other vortex characteristics parameters is presented.

3.3 Vortex core: shape and rotation

In Figures 11 and 12, average vortex core radii are plotted in 36 directions around the centre for different Reynolds numbers, plane locations and angles of attack. These polar plots give an insight into the average vortex core shape.

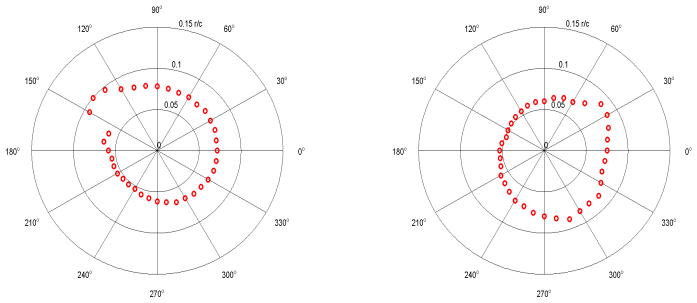

(a) $z/c = 0.25$.

(b) $z/c = 0.5$.

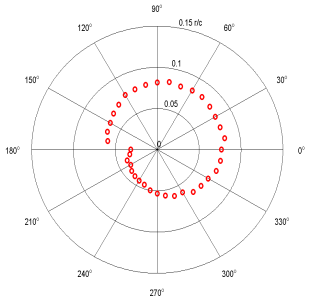

(c) $z/c = 1$.

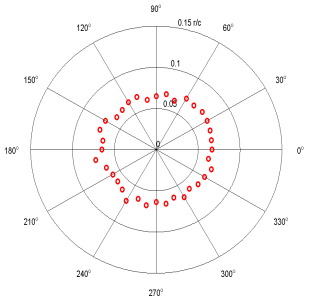

(d) $z/c = 2$.

Figure 11: Vortex core shape at $Re = 1 \cdot 10^5$ and $AoA = 12°$.

In the present reference system, the vortex rotates clockwise and the ones plotted are where a spiral structure of the core is better observed (it is anyway observed in all the cases). The discontinuity is due to the switch

of the maximum tangential velocity (that is at the core radius) between the two peaks discussed previously. At two chords from the wing the vortex seems to have already reached a good axisymmetry for all the cases. In Figures 13, the comparison of the vortex core shapes for different Reynolds numbers at one chord and $12°$ angle of attack is reported. The two high Reynolds number cases show an almost identical pattern where the low Reynolds core shape is similar but with a phase difference of $90°$.

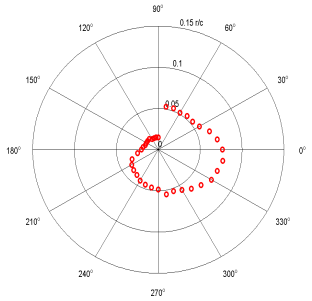

(a) $z/c = 0.25$.

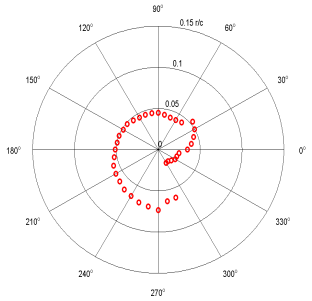

(b) $z/c = 0.5$.

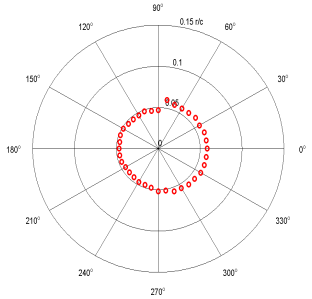

(c) $z/c = 1$.

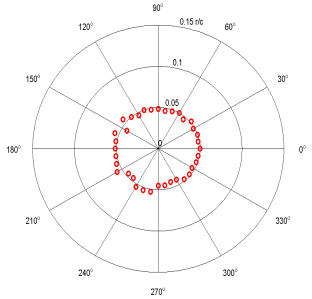

(d) $z/c = 2$.

Figure 12: Vortex core shape at $Re = 5 \cdot 10^5$ and $AoA = 8°$.

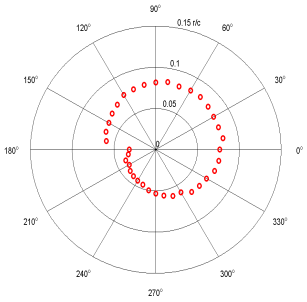

(a) $Re = 1 \cdot 10^5$.

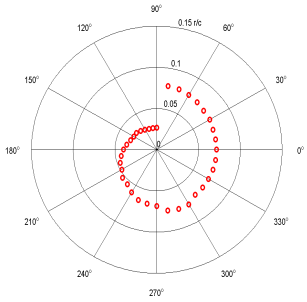

(b) $Re = 5 \cdot 10^5$.

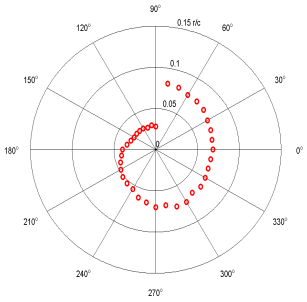

(c) $Re = 10 \cdot 10^5$.

Figure 13: Vortex core shape at $AoA = 12°$ and $z/c = 1$.

From these polar plots is possible to retrieve information on the rotation of the vortex. Because the initial stage is not yet axisymmetric but it reveals a peculiar spiral structure, it is possible to evaluate the rotation of the core following the discontinuity. The vortex core rotation Θ can be then compared with an estimate based on the average around the core at the maximum tangential velocity $v_{t,max}$ (that is approximately the velocity

of the points in the polar plots), the core radius R and the convection driven by the axial velocity w_{core} in a region of the order of the core size. In fact, the rotation can be expressed by an angular velocity multiplied by the time elapsed between two planes translated along the z axis (see Fig. 2):

$$\Theta = \omega \cdot t = \left(\frac{v_{t,max}}{R}\right) \cdot \left(\frac{\Delta z}{w_{core}}\right) \tag{2}$$

The axial velocity is evaluated from Fig. 14 where the averaged axial velocity component has been plotted as function of the radius at the different plane positions. For these plots (i.e. axial velocity studies), the axial velocity aperiodicity correction method has been found to be more accurate and leading to more peaked profiles and higher gradients near the centres.

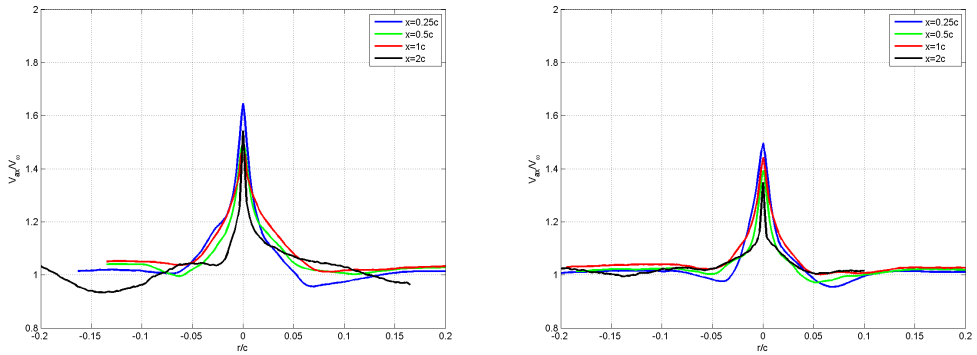

(a) $Re = 1 \cdot 10^5$, $AoA = 12°$. (b) $Re = 5 \cdot 10^5$, $AoA = 8°$.

Figure 14: Axial velocity profiles as function of the radius.

In Tab. 2 the different terms and the resulting core rotations are reported: the initial and ending plane of the range and the related distance Δz covered by the vortex; the maximum tangential velocity $v_{t,max}$ of the mean profile, the mean core radius R and the resulting the mean core angular velocity ω; the core axial velocity w_{core} evaluated as the mean value in the region $0 < r < 3/2\,R$ and the elapsed time t between the two planes of the range; the core rotation Θ. The tangential and axial velocities on one plane have been taken as constant on the range supported by the fact that these values do not change significantly. For example, the values at $z/c = 0.5$ are the values of the range $0.25 < z/c < 0.5$.

$\boldsymbol{Re = 1 \cdot 10^5,\ AoA = 12°}$			
$\boldsymbol{range/c}$	0-0.25	0.25-0.5	0.5-1
$\boldsymbol{\Delta z/c}$	0.25	0.25	0.5
$\boldsymbol{v_{t,max}/U_\infty}$	0.686	0.684	0.704
$\boldsymbol{R/c}$	0.070	0.067	0.070
$\boldsymbol{\omega\ (rps)}$	12.84	13.28	13.18
$\boldsymbol{w_{core}/U_\infty}$	1.08	1.07	1.11
$\boldsymbol{t(ms)}$	28	28	55
$\boldsymbol{\Theta\ (deg)}$	**130**	**135**	**260**

Table 2: Core rotation estimation: $Case\,1$.

$\boldsymbol{Re = 5 \cdot 10^5,\ AoA = 8°}$			
$\boldsymbol{range/c}$	0-0.25	0.25-0.5	0.5-1
$\boldsymbol{\Delta z/c}$	0.25	0.25	0.5
$\boldsymbol{v_{t,max}/U_\infty}$	0.473	0.500	0.499
$\boldsymbol{R/c}$	0.055	0.052	0.050
$\boldsymbol{\omega\ (rps)}$	56.36	62.41	65.38
$\boldsymbol{w_{core}/U_\infty}$	1.05	1.06	1.09
$\boldsymbol{t(ms)}$	5.8	5.7	11.2
$\boldsymbol{\Theta\ (deg)}$	**117**	**129**	**263**

Table 3: Core rotation estimation: $Case\,2$.

Although Eq. (2) comes from rough and preliminary considerations and treats the core spiral structure as in solid axisymmetric rotation, the results are not that distant from polar plots.
Looking at the polar plots of $Case\,1$ (Fig. 11), a peak in the core radius is observed around and angle of $150°$ at $z/c = 0.25$ and it is also observed around an angle of $30°$ at $z/c = 0.5$. The vortex rotates clockwise therefore a rotation of around $120°$ is observed where the Tab. 2 shows a rotation of $135°$. A similar structure is also observed at $z/c = 1$ with a rotation of about $210°$ with a calculated one of $260°$. At 2 chords, as observed earlier, there is no memory of the vortex rolling up phase.

About $Case\,2$ (Fig. 12), a clockwise rotation of the spiral structure is observed in the polar plots between $z/c = 0.25$ and $z/c = 0.5$ of about $150°$ compared to a calculated one of $129°$. From 0.5 to 1 the rotation is observed of $210°$ and calculated of $260°$.
A good agreement is observed between the observations and the results from Eq. (2). In this way, a link between the travel of the vortex and its rotation is found, showing that in around 3 full rotations of the core an axisymmetric condition is achieved.
In a similar way, an initial position of the spiral can also be estimated and it can be placed with the high radius region at about $240°$ as schematically sketched in Fig. 15 where the wing tip is also plotted. This shape suggests a direct link between the high radius region and the high velocity crossing flow (from the pressure to the suction surface of the wing) forced by the abrupt geometry of the square tip.

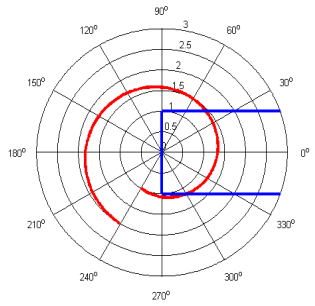

Figure 15: Typical core spiral structure at $z/c = 0$ for a square wing tip.

Re	AoA	$\Theta_{0\to1}$
$1 \cdot 10^5$	4°	349°
$1 \cdot 10^5$	8°	459°
$1 \cdot 10^5$	12°	525°
$1 \cdot 10^5$	15°	576°

Table 4: Core rotation estimation for the range $0 - 1\,c$.

In tab. 4, the vortex rotation in the range between the trailing edge and 1 chord has been evaluated as function of the angle of attack. As expected, an increase of the angle leads to a sensible increase in the rotation (which corresponds to an increase in the angular velocity). Increasing the angle of attack, the lift on the wing increases and so increases the pressure difference between the bottom and the upper surface of the wing resulting in a higher driving force for the tip crossing flow.

3.4 Comparison with the Batchelor vortex

A description of an axisymmetric wake vortex far downstream of an aircraft was presented by Batchelor[3]. The tangential velocity v_t as function of the distance from the centre r is described by the Eq. (3) and plotted in Fig. 16a.

$$v_t = \frac{\bar{\Gamma}}{2\pi r}\left(1 - e^{-r^2/\bar{R}^2}\right) \tag{3}$$

$\bar{\Gamma}$ represents the overall circulation of the vortex, the vortex core radius or inner core (where the tangential velocity reaches the maximum) is $R = 1.12\bar{R}$ and the outer core (where the vortex circulation reaches the asymptotic value[7]) is of the order of $2R$ (see Fig. 16b). The radial component of velocity is zero everywhere. For a typical case, the circulation and the tangential velocity profiles are plotted in Fig. 17. It is seen that the circulation has not yet reached an asymptotic value after 4 core radii but it slowly grows; this can be attributed to the fact that the boundary layer has not yet fully rolled up. The oscillation at large radii is due to the lower quality of the laser sheet at the edges resulting in a lower velocity calculation accuracy. However, the profiles are very similar to the analytical profiles of the Batchelor vortex in Fig. 16 and the use of this analytical vortex as description of tangential velocity of a trailing vortex is a good approximation also in the near field.
An attempt to establish the laws governing the flow in a turbulent line vortex has been made by Hoffmann et al.[10] and further studied by Phillips[15] who experimentally confirmed the universal behaviour of the inner vortex flow and the presence of three regions where shear stresses, Reynolds stresses and inertia terms are differently balanced. Even though the vortex is not truly axisymmetric and the rollup process is not complete, plotting the core values dimensionless circulation on a semi logarithmic chart as function of the core radius dimensionless radial variable, reveals the presence of those regions. An inner region at solid body rotation with small shear stresses and dominating tangential inertia forces; a region near the tangential velocity peak where the tangential inertia forces are small but shear stresses are large and logarithmic distribution of circulation is

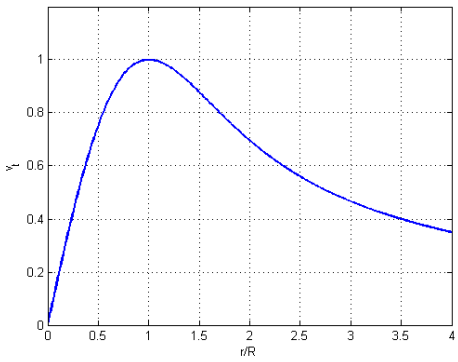

(a) Tangential velocity profile.

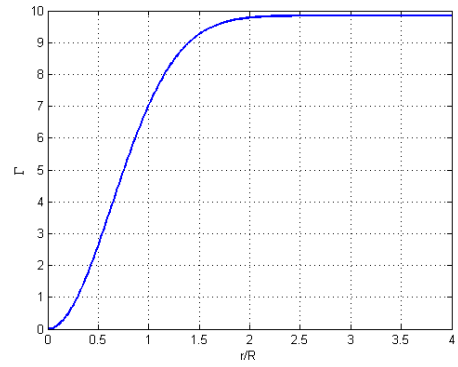

(b) Circulation profile.

Figure 16: Batchelor vortex.

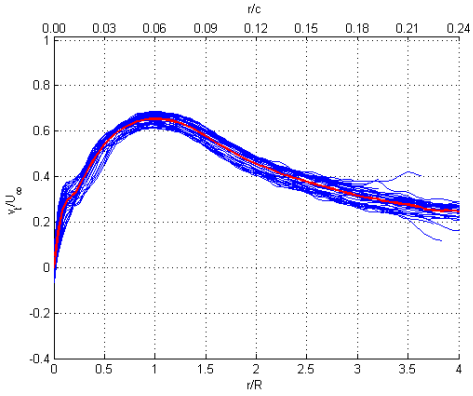

(a) Tangential velocity profile.

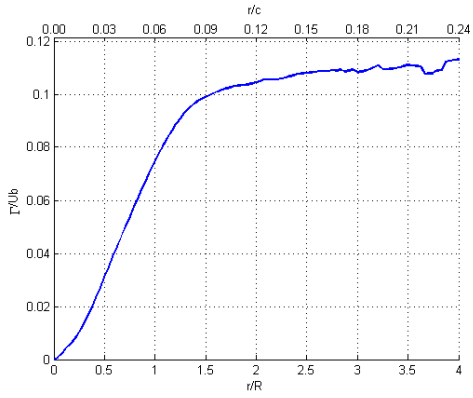

(b) Circulation profile.

Figure 17: $z/c = 2$, $Re = 5 \cdot 10^5$, $AoA = 12°$.

found; an outer core region where a not necessarily universal circulation defect law exists although it remains approximately constant. Whether the outer region is universal or not is yet not clear (see [15], [4] and [22]). The circulation distributions in the first two regions have been expressed as[10]:

$$\begin{aligned} \Gamma(r)/\Gamma_R &= A(r/R)^2 \qquad r/R < 0.4 \\ \Gamma(r)/\Gamma_R &= B\log(r/R) + C \quad 0.5 < r/R < 1.4 \end{aligned} \tag{4}$$

with Γ_R the circulation at the core radius and A, B and C constants. The values of these constants are derived experimentally and slightly differs case to case. An universality in this sense is still to be found. The values of the constants found by Hoffmann[10] and adopted for the red lines in the following plots are:

$$A = 1.83; \quad B = 1; \quad C = 1. \tag{5}$$

In Fig. 18 a dimensionless form of the circulations of all the tests $(\Gamma/U_\infty b)/\Gamma_R$ have been plotted. It is observed that the inner region differs from the curve because the influence of the asymmetry due by the initial roll up phase. It is also observed that the logarithmic region is well described by the curve and the outer region data are very scattered. The profiles that seem to lie more on the logarithmic curve are those cases at low angles of attack where the secondary inflections become higher then the primary one resulting in a convergence reached at much higher dimensionless radius from the centre.
In Fig. 19 the circulation of the Batchelor vortex described in Eq. 3 has also been plotted in logarithmic scale along with the Eqs. 4 and constants as Eq. 5. A very good agreement of these constants also with the Batchelor vortex is observed. The constant circulation value in the outer region has not been found in the experiments and, as said earlier, it can be attributed to the nearness of the studies to the model and the consequent not fully development of the vortex.
Fig. 20 is a zoom in the outer region of the experimental circulations at low Reynolds number where the different colours highlight the angle of attack effect. Even though the oscillations on the profiles are high and

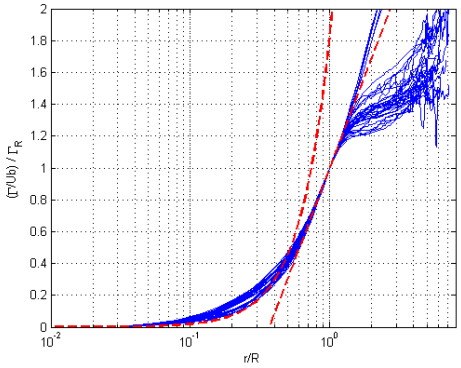

Figure 18: Experiments circulation.

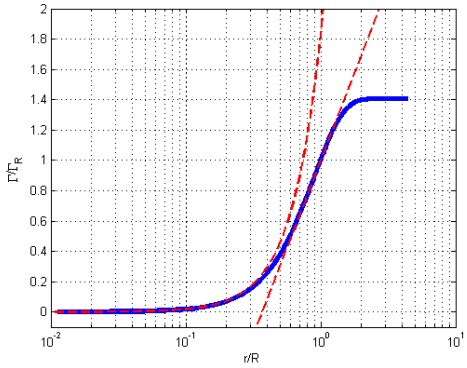

Figure 19: Batchelor vortex circulation.

tend to invalidate the reliability of the results, a relationship between the dimensionless asymptotic value and the angle of attack can be observed.

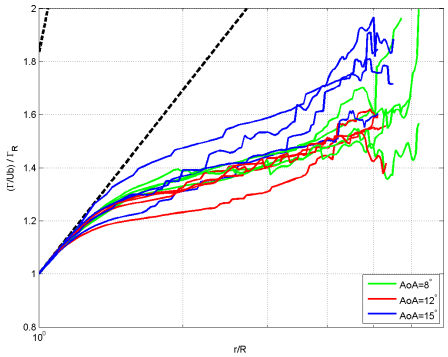

Figure 20: Circulation profiles at $Re = 1 \cdot 10^5$.

4 Conclusions

Particle Image Velocimetry technique has been adopted for a high spatial resolution study on the near field wing tip vortex evolution and development from a high aspect ratio NACA 0015 model with square tip at various Reynolds numbers and angles of attack. An examination of the vortex wandering and of the tangential velocity profiles has provided the following conclusions:

- Vortex wandering is responsible of apparent turbulence and its influence on typical turbulent measurements is in progress. Therefore, shifting the instantaneous vector fields before computing the average is important to separate the proper vortex movement and the effects of the turbulence (and to correctly calculate the Reynolds stresses).

- The helicity peak has been found to be the best aperiodity correction method in a particular way at low angles of attack where an intermittent and very unstable structure of the vortex core is found as consequence of strong secondary vortices.

- The rms values of the vortex centre fluctuations show an increase with the angle of attack at the exception of the incidence of $4°$ where the strong satellite vortices are observed with intensities that are comparable with the primary vortices intensities.

- A double inflection in the tangential profiles is observed in the near wake and addressed as one of the secondary vortices effects. This leads to a strong asymmetry which is vanished at 2 chords of distance from the trailing edge.

- A spiral structure of the vortex core has been observed and a core rotation evaluation procedure has been tested. The vortex rotation slightly increases with the Reynolds number and sensibly increases with the angle of attack (i.e. vortex strength). The initial roll up stage has been directly linked to the abrupt wing tip geometry.
- A good description of the experimental tangential velocity and circulation has been found in the analytical Batchelor vortex even in the near field. Three distinctive regions have been identified in the core where two of them are well described by analytical curves.

REFERENCES

[1] R J Adrian, *Particle-Imaging Technique for Experimental Fluid Mechanics*, Annual Review Fluid Mechanics, **23**, 1991, 261–304

[2] S C C Bailey, S Tavoularis and B H K Lee, *Effects of Freestream Turbulence on Wing-Tip Vortex Formation and Near Field*, Journal of Aircraf, **43**, 2006, 1282–1291

[3] G K Batchelor, *Axial Flow in Trailing Line Vortices*, Journal of Fluid Mechanics, **20**, 4, 1964, 645–658

[4] D Birch, T Lee, F Mokhatarian and F Kafyeke, *Structure and Induced Drag of a Tip Vortex*, Journal of Aircraft, **41**, 5, 2004, 1138–1145

[5] W J Devenport, M C Rife, S I Lipias and G J Follin, *The Structure and Development of a Wing-Tip Vortex*, Journal of Fluid Mechanics, **312**, 1996, 67–106

[6] K Duraisamy, *Studies in Tip Vortex Formation, Evolution and Control*, PhD Thesis, University of Maryland, 2005.

[7] T Gerz, G Holzapfel and D Darracq, *Aircraft Wake Vortices -A position Paper-*, WakeNet Position Paper, 2001

[8] S I Green, *Fluid Mechanics and its Applications*, Kluwer Academic Publisher, 1995, 427–470

[9] G Haller, *An objective definition of a vortex*, Journal of Fluid Mechanics, **525**, 2005, 1–26

[10] E R Hoffmann and P N Joubert, *Turbulent Line Vortices*, Journal of Fluid Mechanics, **16**, 1963, 395–411

[11] L Jacquin, D Fabre and P Geffroy, *The Properties of a Transport Aircraft Wake in the Extended Near Field: an Experimental Study*, 39th AIAA Aeropace Sciences Meeting & Exhibit, 2001, Reno, NV.

[12] R D Keane and R J Adrian, *Theory of Cross-Correlation Analysis of PIV Images*, Applied Scientific Research, **49**, 1992, 191–215

[13] N J Lawson and J Wu, *Three-Dimensional Particle Image Velocimetry: Error Analysis of Stereoscopic Techniques*, Meas. Sci. Technol., **8**, 1997, 894–900

[14] K W McAlister and R K Takahashi, *Wing Pressure and Trailing Vortex Measurements*, NASA Technical Report 3151, 1991

[15] W R C Phillips, *The Turbulent Trailing Vortex During Roll-Up*, Journal of Fluid Mechanics, **105**, 1981, 451–467

[16] A K Prasad, R J Adrian, C C Landreth and P W Offutt, *Effect of Resoluation on the Speed and Accuracy of Particle Image Velocimetry Interrogation*, Experiments in Fluids, **13**, 1992, 105–116

[17] M Raffel, C Willert, S Wereley and J Kompenhans, *Particle Image Velocimetry: a Practical Guide*, Meas. Sci. Technol., Springer, 2nd, 2007

[18] M Ramasamy, B Johnson, T Huismann and J G Leishman, *Digital Particle Image Velocimetry Measurements of Tip Vortex Characteristic Using an Improved Aperiodicity Correction*, Journal of the American Helicopter Society, **54**, 012004, 2009

[19] F De Souza and D Faghani, *Near-Field Wing Tip Vortex Measurements in PIV*, 19th AIAA Applied Aerodynamics Conference, 2001, Anaheim, CA

[20] W Zang and K Prasad, *Performance Evaluation of a Scheimpflug Stereocamera for Particle Image Velocimetry*, Applied Optics, **36**, 33, 1997, 8738–8744

[21] L Zuhal and M Gharib, *Near Field Dynamics of Wing Tip Vortices*, 31st AIAA Fluid Dynamics Conference & Exhibit, 2001, Anaheim, CA.

[22] B R Ramaprian and Y Zheng *Measurements in Rollup Region of the Tip Vortex from a Rectangular Wing*, AIAA Journal, **35**, 12, 1997